Winter 3-20-2020

THE CRYSTAL STRUCTURE OF (CUXZN1-X)0:456IN1:084GE0:46O3 (CUZIGO) USING NEUTRON AND X-RAY DIFFRACTION

Boluwatife A. Adekoya
DePaul University, ajadekoya@gmail.com

THE CRYSTAL STRUCTURE OF $(CU_XZN_{1-X})_{0.456}IN_{1.084}GE_{0.46}O_3$ (CUZIGO) USING NEUTRON AND X-RAY DIFFRACTION

A Thesis

Presented in

Partial Fulfillment of the

Requirements for the Degree of

MASTER OF SCIENCE

August, 2 0 1 9

BY

AJ Adekoya

PHYSICS DEPARTMENT

College of Science and Health

DePaul University

Chicago, Illinois

TABLE OF CONTENTS

LIST OF FIGURES

LIST OF FIGURES – *Continued*

LIST OF FIGURES – *Continued*

ABSTRACT

The solid solution $(Cu_xZn_{1-x})_{0.456}In_{1.084}Ge_{0.46}O_3$ (CuZIGO) has a complex structure where zinc and copper partially occupy a site shared by indium and germanium. ZIGO, the x=0 endpoint, is a potential transparent conducting oxide (TCO) with similar conductivity and transparency to cubic In_2O_3, which, when doped with Sn^{4+}, is the most prevalent TCO. ZIGO structure possesses a tetragonal structure and has the ability to produce multiple new phases with an array of properties that are beneficial to identify and understand. Analyzing this structure is best done through chemical substitution to identify the newly produced phases. Copper is a suitable choice because of its ability to be easily incorporated into the ZIGO structure and create a complete solid solution between the ZIGO phase and the CIGO $(Cu_xZn_{1-x})_{0.456}In_{1.084}Ge_{0.46}O_3$ phase.

The incorporation of copper in the ZIGO structure was studied using both neutron and x-ray diffraction. Using Rietveld analysis, copper was localized at the 16f site of tetragonal $(Cu_xZn_{1-x})_{0.456}In_{1.084}Ge_{0.46}O_3$. Analysis using both GSAS-II and FullProf displayed a lack of copper in any of the three other cation sites (8e, 4a or 4b, which are occupied by indium, indium, and germanium, respectively in the ZIGO compound). The lattice parameters of the solid solution $(Cu_xZn_{1-x})_{0.456}In_{1.084}Ge_{0.46}O_3$, where x = 0.25, 0.50, 0.75, and 1.00, were investigated with high-resolution synchrotron diffraction data. These lattice parameters decreased as copper increased between x=0.25 and x=0.75, but they increased for x=1.00. The lattice parameter changes indicate that a full solid solution is achieved in this quaternary structure. Implications and challenges on the structural characterization of complex new materials are briefly discussed.

CHAPTER 1

Introduction

1.1 Background

Transparent conducting oxides (TCOs) are materials possessing a combination of high-levels of electrical conductivity and optical transparency in the visible region of light. These TCOs usually peak at a value of 85-90% transmittance. Ideally, these TCOs will also have a resistivity of $5x10^{-5}$ Ω·m.[3] Comparatively, optically transparent objects such as glass fibers are electrical insulators, whereas most semiconductors and metals are opaque and optically resistant. These oxides act as an intermediate option between these two extremes.[1,2] The value of these materials lies in their ability to be used for flat-panel displays, solar cells, and photovoltaic devices.[3,4] By doping these TCOs with certain elements, characteristics such as electrical conductivity and optical transparency can be adjusted, leading to increased opportunity for applications.[1]

Transparent conducting oxides are classified into two main categories: n-type and p-type. In_2O_3 is naturally a semiconductor, which can be doped with Sn to produce n-type indium tin oxide (ITO), a well-known transparent conductor.[3,4] P-type TCOs that have been created in the past have lacked the conductivity of previously studied and made n-type TCOs. However, it is believed that new p-type TCOs could be made by doping oxides with copper and other similar elements. By looking at these p-type TCOs, more applications involving combined n-type and p-type TCOs such as CuZIGO and ZIGO, can be developed.

1.2 Crystallographic Structure of ZIGO

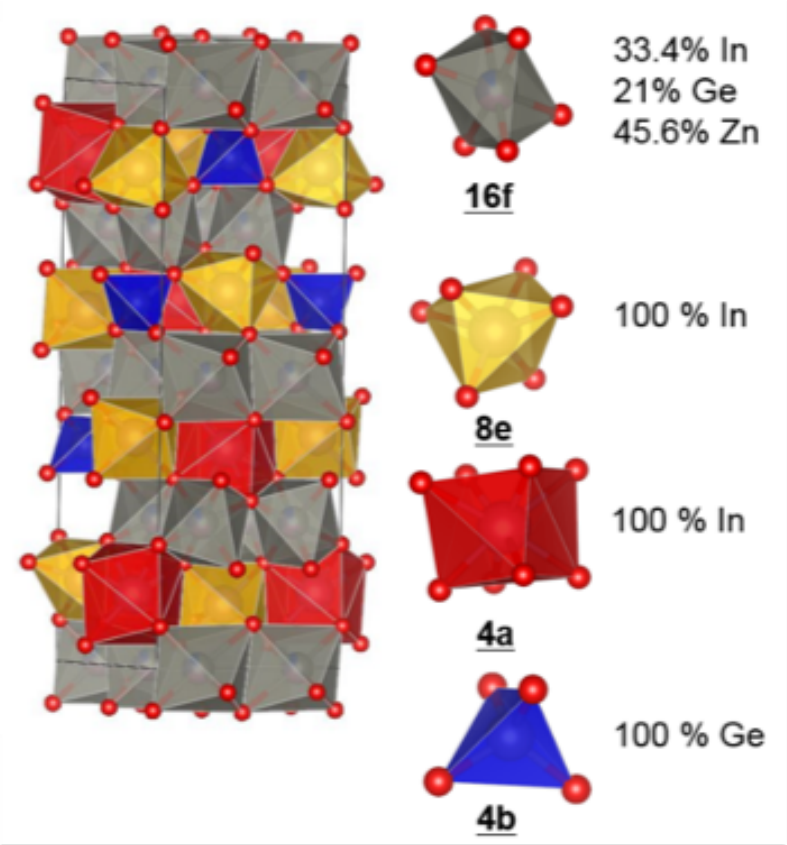

Figure 1.1: (Left) The crystal structure of tetragonal ZIGO. (Right) The four distinct cation sites and their occupancy percentages in ZIGO. [5]

The compound $Zn_{0.456}In_{1.084}Ge_{0.46}O_3$ (ZIGO) has a unique tetragonal structure, shown in Figure 1.1, which is unlike the cubic bixbyite structure of In_2O_3.[5] This bixbyite structure can be seen in Figure 1.2, showing 32 cations in the b and d sites and 48 anions of oxygen. ZIGO holds a structure similar to this with its own 80 atoms, however, the structure must be adapted to fit the extra sites that change the cubic structure of In_2O_3 to the tetragonal structure of ZIGO. The cubic structure has lattice parameters a, b, and c that are all equal. Comparatively, the tetragonal structure has lattice parameters a and b which are equal, but a third side, c, has

a larger length. Both of these crystal structures maintain the same angle of 90° between each side.

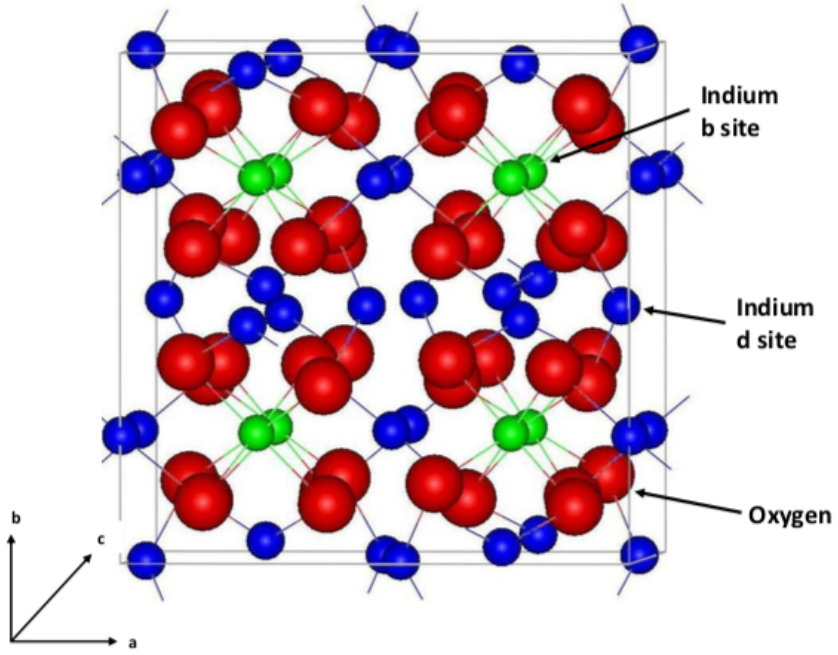

Figure 1.2: Cubic bixbyite structure of In_2O_3. Lattice parameters, a, b, and c are all equal.[6]

Both structures belong to the anion-deficient fluorite family of materials. The ZIGO compound belongs to the crystallographic space group $I4_1/amd$, with unit cell parameters of $a = b = 7.033986(19)$, and $c = 19.74961(8)$ Å.[5] As evidenced by Figure 1.1, ZIGO has four cation sites, 4a, 4b, 8e, and 16f, each differing in their atomic makeup, which are detailed in Table 1.1. There are also 3 anion sites that are each filled fully by oxygen, which are all denoted as the 16h site. These sites are known as Wyckoff sites. Each Wyckoff site has a number which details the number of atoms present when that site is fully occupied. For each space group, the site with the highest symmetry has the smallest multiplicity (number of atoms in the site) and is assigned the Wyckoff letter "a." As the symmetry decreases, the multiplicity

increases, and the letters follow the alphabet. Looking at ZIGO, the 4a and 4b sites have four total atoms that are all indium and germanium respectively, and are the sites with the highest symmetry. The 8e site has 8 atoms of indium. The 16f site has 16 atoms of indium, germanium, and zinc, collectively. The 16h sites are fully occupied with oxygen and have the lowest symmetry of all sites in CuZIGO. These sites along with the occupancy of each atom and the atomic positions are summarized in Table 1.1.[7]

Atom	Occupancy	Site	x	y	z	Uiso
In1	100% In	4a	0	-0.25	0.125	0.0222(3)
Zn/In/Ge	0.456/0.334/0.21	16f	0.2267(1)	0	0	0.0168(2)
In3	100% In	8e	0.5	0.25	-0.10483(3)	0.0139(2)
Ge1	100% Ge	4b	0.5	0.25	0.125	0.0065(3)
O1	100% O	16h	0.0287(5)	0.0697(2)	0.0115(8)	
O2	100% O	16h	0.5	0.0483(5)	0.0729(2)	0.018(1)
O3	100% O	16h	0.2523(7)	0.25	-0.0356(2)	0.026(1)

Table 1.1: Atomic sites and occupancies of ZIGO. The x, y, z values correspond to fractional coordinates in a unit cell. Uiso corresponds to the isotropic atomic displacement parameters, which are related to atomic thermal motion.[5]

1.3 Motivation for Studying CuZIGO

In the field of transparent conducting oxides, there are well-studied and known compounds, such as indium oxide and zinc aluminum oxide. ZIGO is a new transparent conducting oxide (TCO), with a possibility for new applications. It is important because of the information it provides to learn about new, undiscovered solid solutions and transparent conducting oxides. The role of TCOs in flat-panel displays and photovoltaic devices lies in their unique set of characteristics, both optically and electrically.[5] Most TCOs consist of a combination of an oxide with indium, gallium, tin, cadmium and/or zinc. In_2O_3 (indium oxide), the most common

TCO, has a cubic, bixbyite structure, as seen in Figure 1.2, and lattice parameters of 10.117Å for a, b, and c.[8] Comparative to ZIGO's tetragonal lattice parameters of 7.034Å for a and b, and 19.749Å for c. When indium oxide is doped with tin, this structure adjusts by increasing the lattice parameter to allow tin to substitute into the indium sites, without changing the cubic bixbyite structure.[8] A primary goal for studying CuZIGO is to determine if copper will act similarly when it is incorporated into ZIGO.

Currently, the conductivity of ZIGO is assumed to be based off the stoichiometry between Ge and Zn. Copper compounds have potential p-type TCO properties.[9] Though mostly unknown, an important aspect of these p-type TCOs is their similar level of optical and electrical effectiveness as n-type TCOS. Generally, n-type TCOs have a transmittance of about 80-90%, but p-type TCOs have the potential to be completely transparent.[10] Also having p and n-type TCOs opens up more applications for these materials such as p-n junctions, which are a conjoining of n-type and p-type semiconductors. These areas of charge equilibrium cause a potential difference across the junction from the n-type semiconductor to the p-type semiconductor leading to a buildup of voltage between the two semiconductors. This developed electric field prevents any influx or outflux of electrons leading to an equilibrium state in the system.[11]

CHAPTER 2

Experimental Methods

To begin the studying of the crystal structure of CuZIGO, samples were synthesized by the Poeppelmeier group at Northwestern University. Diffraction data for the synthesized samples were measured at the Advanced Photon Source (APS) at Argonne National Laboratory, at the High Flux Isotope Reactor (HFIR), and at the Spallation Neutron Source (SNS) at Oak Ridge National Laboratory.

2.1 Synthesis by the Poeppelmeier Group at Northwestern University

Four CuZIGO samples $(Cu_xZn_{1-x})_{0.456}In_{1.084}Ge_{0.46}O_3$ (x=0.25, 0.50, 0.75, and 1.00) were synthesized with high-temperature solid-state reactions. Cu_2O (Alfa Aesar, 99.9%), In_2O_3 (Alfa Aesar, 99.994%), GeO_2 (Sigma Aldrich, 99.998%), and ZnO (Alfa Aesar, 99.9%) were ball milled with agate media for four, 15-minute cycles at 450 rpm. Powders were pressed into 13 mm diameter cylindrical pellets and individually buried in excess powder, with the same composition as the samples, in triply nested-alumina crucibles to suppress preferential loss of Zn and Cu owing to volatilization. Samples were heated to 1250°C at 5°C per min, held for 16 hours, and then cooled to room temperature at 10°C per min. Lower reaction temperatures (1150°C) were used for the highest Cu-content sample to prevent excessive evaporation during the reaction.[12] For x-ray synchrotron measurements, small amounts (<1 gram) were prepared. For neutron measurements, several batches of x=0.50 and x=0.25 were prepared and combined to obtain 2-3 grams per sample.[12]

2.2 Rietveld Refinement Theory

The structure of CuZIGO was determined from X-Ray powder diffraction at the Advanced Photon Source (APS) at Argonne National Laboratory and neutron diffraction data from the HFIR facility and SNS at Oak Ridge National Laboratory. The diffraction data were then analyzed using two different refinement programs. FullProf Suite[13] and General Structure Analysis System II[14] both use Rietveld refinement, which allow users to study diffraction data from laboratory and synchrotron x-rays in addition to constant wavelength and time-of-flight neutron data.

Rietveld refinement is a method developed by Hugo Rietveld in 1969[15] to analyze powder diffraction data. The method uses a least-squares fit between observed and calculated scattered intensities.[13] Using peak shape, width, and position parameters, the Rietveld refinement is able to calculate intensities that are then compared to observed intensities and used to determine the "goodness-of-fit." This knowledge is used to identify structural characteristics of the powder diffraction pattern.[13]

2.2.1 Bragg's Law

Using Bragg's Law, the d-spacing of atomic planes can be determined. Equation 2.1,

$$n\lambda = 2d\sin\theta \tag{2.1}$$

is used in a diffraction experiment to determine the d-spacing using values of incident (x-ray, neutron, or electron) wavelength, λ, the order of reflection, "n", and the angle of incidence, θ. The wavelength of the radiation and the theta range are experimental parameters determined by the diffractometer that is used. The lattice parameters, a and c, are determined from the d-spacing, "d," and the Miller indices,

h, k, and l. These Miller indices illustrate the orientation of a plane in the crystal structure.

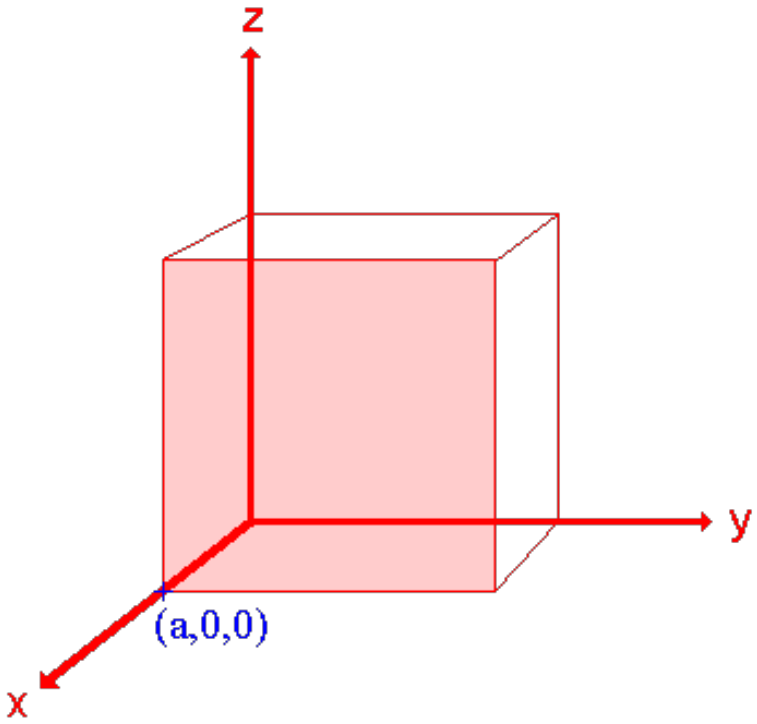

Figure 2.1: Figure displaying an example of the Miller Indices. The Miller indices are found by taking the inverse of points that intersect the fractions of the unit cell in x,y,z. In this example, the intersection points for x, y, z are a, 0, 0, with a=1.Therefore, the shaded area corresponds to the (100) plane. [16]

The reciprocal of the fractional value of the intersection point between the planes and the x, y, and z axes determines the Miller indices. If the plane never intersects an axis, then the intersection point is infinity, and the reciprocal will then give a Miller index of zero for that axis. In Figure 2.1, the intersection point for x is at point "a," where $a = 1$. Using this, the fractional value would be 1/1, leading to a reciprocal value of 1. For y and z, the intersection point is ∞, so the reciprocal

would be 0. This is why in Figure 2.1, the Miller index would be (100). Once Miller indices have been determined, Equation 2.2 can be used to determine the lattice parameters for a tetragonal unit cell like CuZIGO.[16,17]

$$\frac{1}{d^2} = \frac{h^2 + k^2}{a^2} + \frac{l^2}{c^2} \tag{2.2}$$

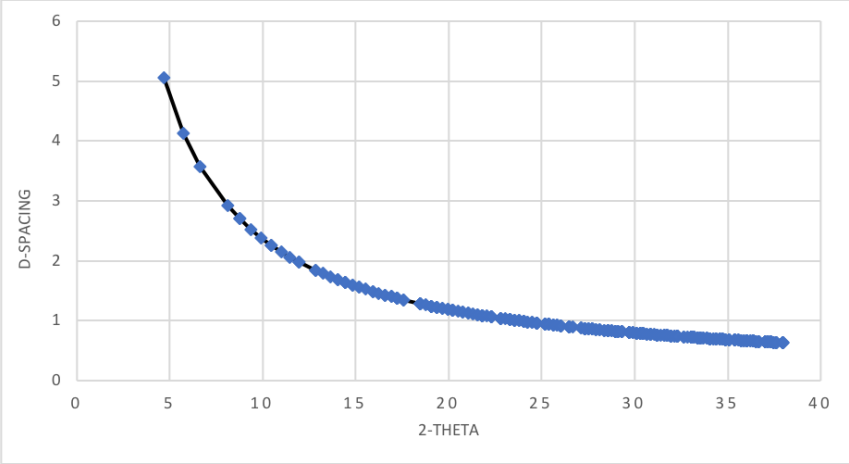

Figure 2.2: Graph displaying the d-spacing versus 2θ values. For each 2θ value, there is a d-spacing value, corresponding with a particular set of Miller indices and a set of lattice parameters. Because these data were gathered from 11-BM, the wavelength value used is 0.41267 Å.

Using peak positions, GSAS uses equation 2.2 to determine the lattice parameters. Each d-spacing value is associated with a particular set of Miller indices. As seen in Figure 2.2, each 2θ value, which is used to graph peak positions, also corresponds to a d-spacing value. By inputting this information into equation 2.2, a set of lattice parameters, a and c, can be determined. These lattice parameters can then be averaged out to create a value for a and c, which will be used to represent a unit cell.

2.2.2 Intensity Calculations

The pattern can be given as a set of two arrays, $\{\mathrm{T}_i,\mathrm{y}_i\}_{i=1,\ldots,n}$, where T_i is a discrete set of 2θ scattering angles, and y_i is the intensity at a given point i. The calculated intensity at any ith point can be written as,

$$y_{c,i} = \sum_{\phi} S_{\phi} \sum_{h} I_{\phi,h} \Omega(T_i - T_{\phi,h}) + b_i \tag{2.3}$$

where h corresponds to the Bragg reflections and b_i is the background intensity. The subscript ϕ corresponds to the existing phases, which vary from 1 to the total number of crystallographic phases found in the sample. S_{ϕ} is the scale factor of the phase, and Ω is the function consisting of both instrumental and sample effects. $\mathrm{I}_{\phi,h}$ is the integrated intensities at a point i due to reflection h and is written as,

$$I_{\phi,h} = \{LAPCF^2\}_{\phi,h} \tag{2.4}$$

where A denotes the absorption correction, and P is the preferred orientation function. L contains the Lorentz polarization and multiplicity factors, while F represents the structure factor. C contains special corrections, including non-linearity, efficiencies, special absorption corrections, extinctions, etc.

2.2.3 Goodness-of-Fit

The Rietveld Method consists of refining a crystal structure using a minimized weighted square difference between the observed and calculated peak intensities. This is referred to as the "chi-squared" function or "goodness-of-fit,"

$$\chi^2 = \sum_{i=1}^{n} w_i \{y_i - y_{c,i}(\alpha)\}^2 \tag{2.5}$$

where $w_i = \frac{1}{\sigma_i^2}$ with σ_i^2 defined as the variance of the observation "y_i". The intensities are matched against the parameter vector α=(α_1,α_2,α_3,α_4,...). This chi-squared

value is then reduced by the following expression:

$$\chi_V^2 = \left[\frac{R_{wp}}{R_{exp}}\right]^2 = S^2 \tag{2.6}$$

with S being the "goodness-of-fit." R_{wp} is the weighted profile factor and is defined as:

$$R_{wp} = 100\left[\frac{\sum\limits_{i=1,n} w_i|y_i - y_{c,i}|^2}{\sum\limits_{i=1,n} w_i y_i^2}\right]^{\frac{1}{2}} \tag{2.7}$$

R_{exp} is defined as expected weighted profile factor and expressed as

$$R_{exp} = 100\left[\frac{n-p}{\sum\limits_{i} w_i y_i^2}\right]^{\frac{1}{2}} \tag{2.8}$$

where $n-p$ is defined as the degrees of freedom, with n being the number of total points used in the refinement, and p being the total number of refined parameters.[13]

2.3 Neutron Diffraction

Neutron diffraction patterns were collected at HFIR using a wavelength of 1.539300Å. The measurements were all done at room temperature, although the diffractometer can measure samples at temperatures up to 1800K. The HB-2A diffractometer has a scattering angle range, 2θ, of 2° to 155°, as well as a minimum d-spacing of ∼0.8 Å. It also has a resolution of $2*10^{-3}$ Δd/d allowing for more narrow, accurate peaks at large scattering angles. Since large quantities (∼2g) of powder are needed for neutron diffraction experiments, several batches of only two compositions (x=0.25 and x=0.50) were prepared.

Neutron samples were also sent to the SNS to collect data using the POWGEN diffractometer. This diffractometer provides a much higher resolution measurement that can be used for Rietveld analysis. Some of this resolution can also be traded

in for intensity allowing shorter measurements to be taken at very good resolutions. POWGEN also uses a high-resolution range of $8 * 10^{-4} - 2.5 * 10^{-3}$ Δd/d and a *d*-spacing range of 0.1-8Å for single measurements. Similar to the measurements taken at HB-2A, these measurements were also taken at room temperature.

Element	Neutron Bound Coh (fm)	Atomic Number
Oxygen (O)	5.803	8
Germanium (Ge)	8.42	32
Indium (In)	4.065-0.539i	49

Table 2.1: Neutron scattering lengths of the relevant elements and their associated atomic numbers, which are related to the x-ray scattering factors.

Neutron diffraction scattering lengths are different from x-ray scattering factors, which are proportional to the number of electrons. X-ray diffraction techniques are more common than their neutron diffraction counterparts. Because these x-ray diffraction techniques have been used for so long, they are also easier to optimize, resulting in more trusted results, especially when using x-ray synchrotron techniques. However, x-ray techniques depend on the atomic number of the elements being studied. As seen in Table 2.1, normally elements studied have varying atomic numbers so studying these elements can be done easily. In cases similar to CuZIGO, where two elements have similar atomic numbers (*e.g.* copper and zinc), it is difficult to differentiate between the two elements. However, the difference between their neutron scattering lengths is much greater, as can be seen in Table 2.2. The percent difference between the x-ray scattering power of elements are too close to one another, so the study of these particular elements via neutron diffraction can provide meaningful results. Furthermore, the study of oxides via neutron diffraction is recommended since light elements, such as oxygen, have strong scattering power.

	Copper (Cu)	Zinc (Zn)
Atomic Number	29	32
Neutron Scattering Length	7.718	5.68
Percent Difference (x-ray)	10.3	
Percent Difference (neutron)	26.4	

Table 2.2: X-ray scattering power and neutron scattering length comparison between copper and zinc detailing the differences between the two methods.

2.4 X-Ray Diffraction

Since x-ray laboratory sources are common and relatively inexpensive, the first step in identifying crystallographic phases usually consists of using a lab source. X-ray synchrotron data have better resolution and higher statistics in comparison to both x-ray laboratory and neutron sources. Both x-ray and neutron data allow the identification and quantification of secondary crystallographic phases in samples. However, unlike neutron diffraction, light elements such as oxygen, nitrogen, and fluorine are weak scatterers, so obtaining information about these elements is not possible using only x-ray diffraction.

For this study, synchrotron x-ray powder diffraction patterns were collected using beamline 11-BM at the APS. The patterns were collected over a 2θ range of 10-60° at a wavelength of 0.41267Å, a minimum d-spacing of ∼0.54Å, and at a temperature of 300 K. The beamline uses a high resolution of $1.4 * 10^{-4}$ Δd/d for data collection. Lattice parameters and atomic coordinates were obtained by Rietveld refinement using the General Structure Analysis System II[14] package and the FullProf Suite[13]. All four samples of x=0.25, 0.50, 0.75, and 1.00 were analyzed using x-ray diffraction. 11-BM data were also collected on the second set of samples of x=0.25 and x=0.50 that were measured using neutron sources.

2.5 GSAS II

Using General Structure Analysis System II (GSAS II), analyses of the neutron diffraction data (ND) and x-ray diffraction data (XRD) were performed. GSAS II is a software package that can be used for data reduction, structure solution, crystallographic analysis, small-angle scattering analysis, and more. It employs the Rietveld refinement method using the least-squares fit between calculated and observed intensities for XRD and ND. GSAS II processes the diffraction pattern reflection by reflection in order to find calculated intensities of the peaks. These calculated intensities, y_c, are matched with $\partial y_c/\partial p_i$, in a Jacobian matrix. This gives the step-by-step function creating peak values, which are used to characterize the solution structure.[14]

GSAS II provides the user with the ability to adjust and control most of the parameters given. The instrumental resolution function must be entered. It is obtained by refining peak shape parameters using a standard reference material (SRM) obtained from NIST (National Institute for Standards and Technology).[14] In the present study, LaB6 (SRM 660c) and Si(640e) standards were used. The program uses a pseudo-Voigt function to match the peak shape, as a combination of a Lorentz distribution and a Gaussian distribution. In an attempt to get the best possible fit for the peaks, it allows the user to refine sample specific contributions to peak broadening. In this study, ionic x-ray and neutron scattering factors were used. The backgrounds were fitted using 7th-degree Chebyshev polynomials. A sample displacement correction perpendicular to the beam was refined. Atomic positions, isotropic atomic displacement (Uiso) parameters as well as microstrain

and size broadening were refined for each CuZIGO sample.

CHAPTER 3

Results and Discussion of CuZIGO Diffraction

3.1 Rietveld Refinements of CuZIGO using GSAS II

In this chapter, the analyzed diffraction data of CuZIGO will be presented. The possibility of multiple phases and the presence of copper in sites other than the expected 16f site will be discussed. The lattice parameters for each sample after the substitution of copper will also be reviewed. The XRD data were refined using the ZIGO tetragonal structure.

3.1.1 Analysis of x-ray data with Cu occupying only the 16f site

As seen in Figure 3.1, there are 4 cation sites found in CuZIGO. The 4a and 8e sites are completely filled by indium, the 4b site is filled by germanium, and the 16f site is filled by a combination of indium, germanium, zinc, and copper. CuZIGO also has 3 anion sites, which are solely filled by oxygen. One tetragonal unit cell has a total of 80 atoms, similarly to a cubic unit cell of In_2O_3.

Structural information for the x=0 (ZIGO) sample was used as a starting point for the refinements of CuZIGO. Lattice parameters, sample displacements, microstrain, size parameters, and background functions were then refined in the CuZIGO samples and compared to the x=0 sample. As mentioned earlier, the lattice parameters, a and c for the tetragonal cell can be refined from the positions of the peaks in each diffraction pattern. Copper was introduced into the 16f site for the x=0.25, 0.50, 0.75, and 1.0 samples. The lattice parameters obtained from the refined synchrotron x-ray for all four samples, and the x=0 endpoint, ZIGO, can be seen and compared

in Figure 3.2. Each lattice parameter notably shows a gradual decrease as copper concentration increases from x=0 to x=0.75. This is consistent with the decrease in radius from Zn^{2+} to Cu^{2+}.

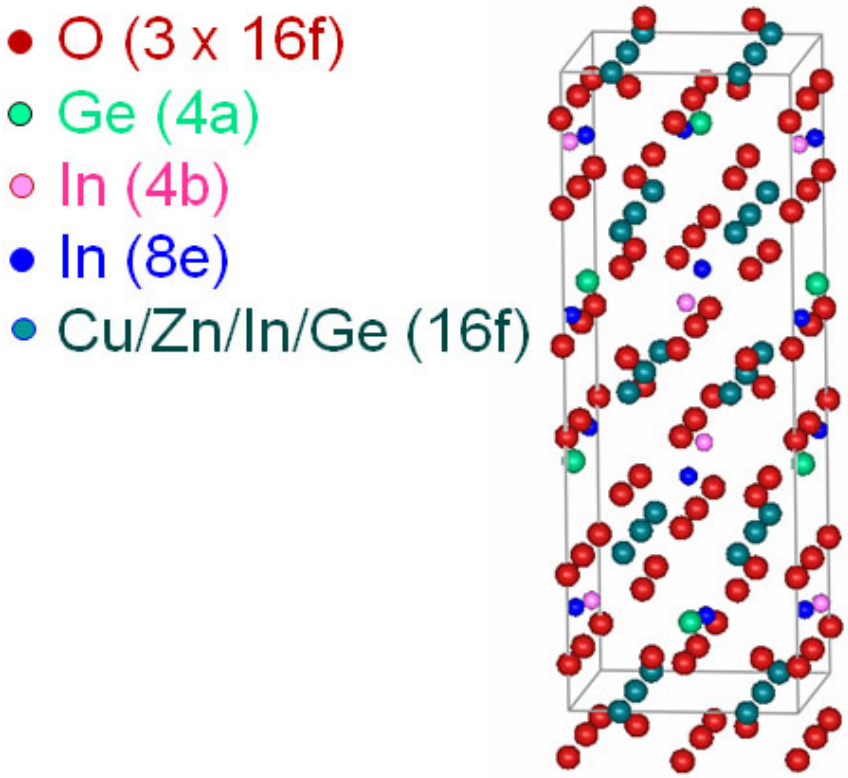

Figure 3.1: Unit cell of tetragonal CuZIGO, space group $I4_1/amd$. There are a total of 32 cations distributed over 4 different sites, and 48 anions occupying 3 sites.

The observed results deviate from the expected behavior that should follow from Vegard's Law for solid solutions, which states that the relation between lattice parameters and concentration should follow a linear relationship.[18] According to Vegard, the role of atomic-size is an important aspect of the changing crystal structure. For CuZIGO, the decrease in zinc concentration is consistent with the decrease in the lattice parameters from the x=0 to 0.75 samples. However, between

x=0.75 and complete substitution, there are increases in the a and c parameters, with the change in c being significantly larger. This deviation from the expected Vegard's Law, has previously been explained in other systems, by potential ordering, clustering, and magnetic effects of the introduced species. The ordering of Cu^{2+} at low values of x may potentially minimize the effect of these penalties. The 16f site allows for the greatest amount of interaction between nearby Cu^{2+} polyhedra. Since the 16f sites are perpendicular to the c-axis, distortion-minimizing interactions would be expected to be on enhanced in the a and b directions. This, combined with the lack of direct connection with the c-direction, would explain the larger expansion in the c-direction compared to the a and b directions. [12,18]

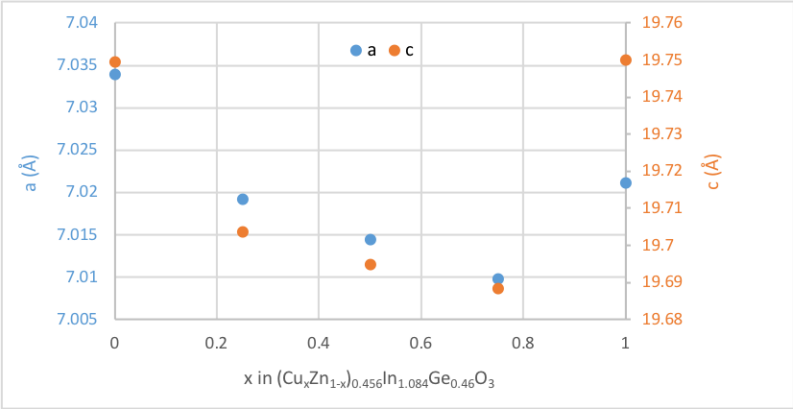

Figure 3.2: Lattice parameters for all phases of CuZIGO x-ray synchrotron data, as a function of Cu concentration (x). x=0 values from Rickert *et al.*[5] x=0.25, 0.50, 0.75, and 1.00 values from refinements done using GSAS II.[14]

Figures 3.3-3.6 display the best Rietveld refinements of CuZIGO. Rietveld refinements of synchrotron XRD data show small amounts of In_2O_3 and $In_2Ge_2O_7$ in the x=0.25 and x=1.00 samples. In Figures 3.3, 3.4, and 3.6, there are 3 phases found in the Rietveld refinement, which make up 100% of the sample. The x=0.75 sample did not show those secondary phases. For both the x=0.75 and the x=1.00 samples, there were peaks whose phases have not been identified.

In a second set of refinements, for all of these samples, Cu was also placed at the 16f site, and was allowed to occupy the 4a, 4b, and 8e cation sties. The results showed that Cu was absent at the 4a, 4b, and 8e sites. As mentioned before, GSAS II calculates an R_{wp} "goodness-of-fit" value after each refinement using Equation 2.7. This R_{wp} value and the refined occupations were used to determine the quality of the fits and decide if Cu should be placed at other cation sites.[14]

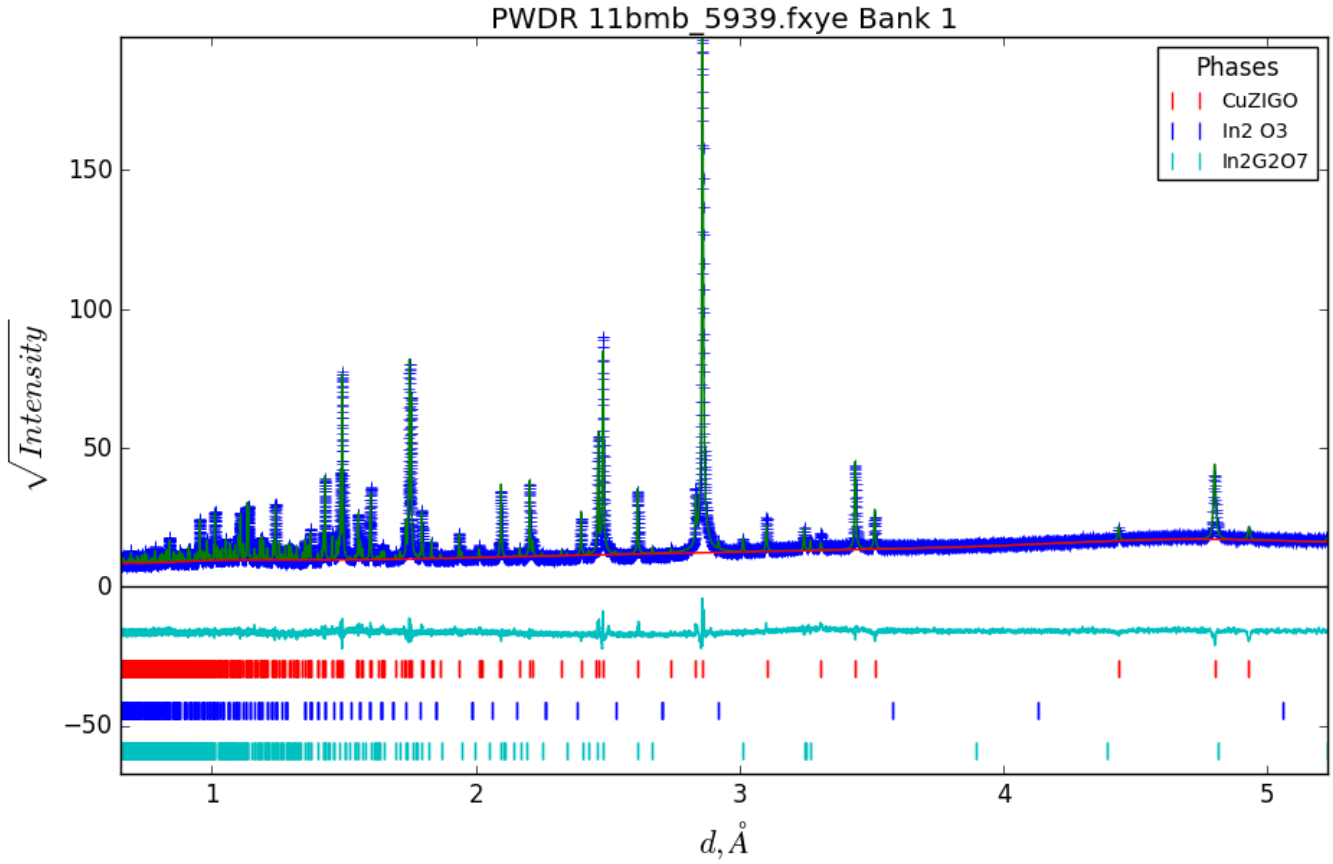

Figure 3.3: Rietveld refinement of XRD for $(Cu_xZn_{1-x})_{0.456}In_{1.084}Ge_{0.46}O_3$ sample x=0.25. The phase distribution is 98.8% CuZIGO, 1.1% $In_2Ge_2O_7$, and 0.1% In_2O_3. In order to see weak diffraction peaks, the y-scale is the square root of intensity. The dark blue points represent the measured diffracted intensity. The green line corresponds to the calculated intensities from Equation 2.3. The cyan line is the difference between the measured and fitted intensity, so a horizontal line would correspond to a perfect fit. The small vertical lines show the "d" positions of the diffraction peaks from each crystallographic phase in the sample.

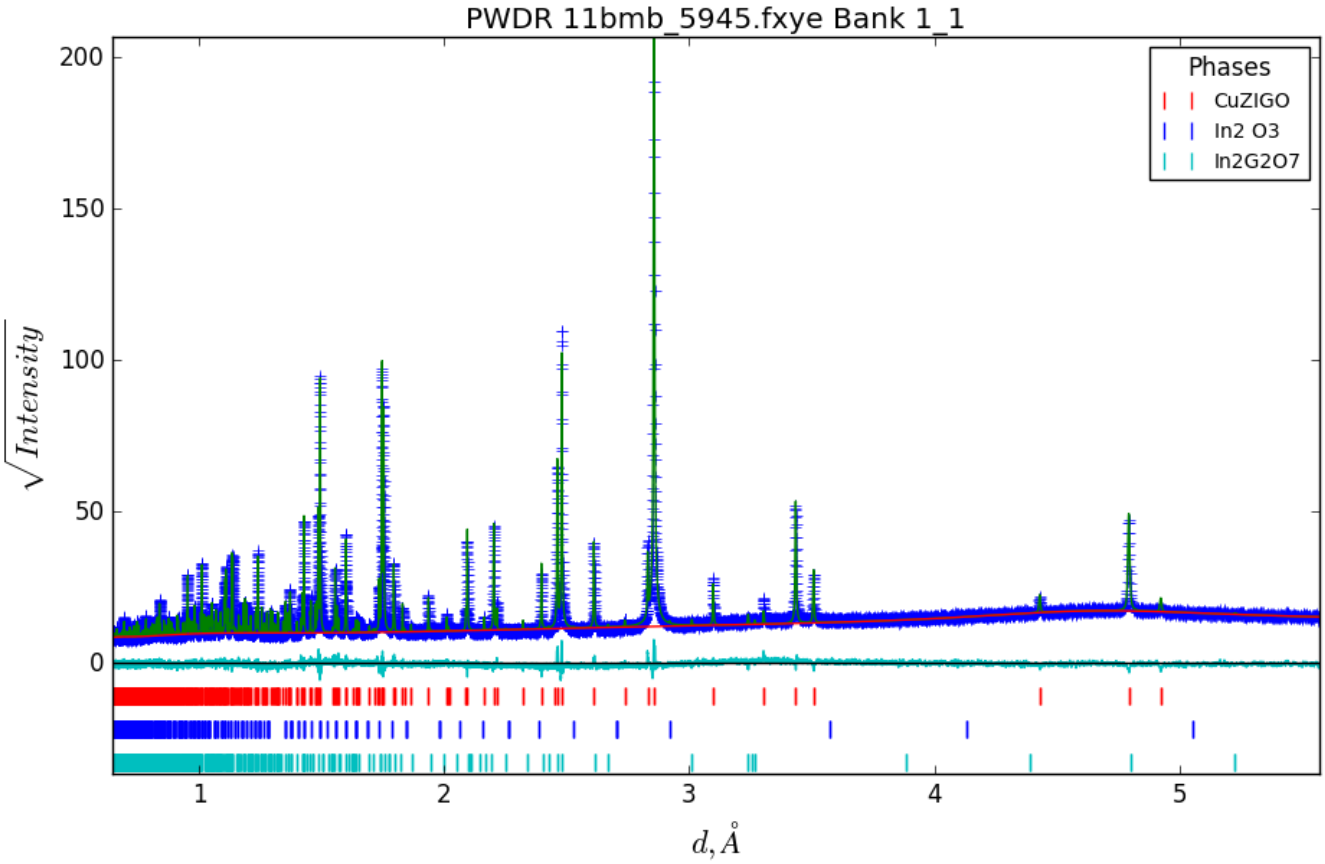

Figure 3.4: Rietveld refinement of XRD for $(Cu_xZn_{1-x})_{0.456}In_{1.084}Ge_{0.46}O_3$ sample x=0.50. The sample is 98.77% CuZIGO, 1.2% $In_2Ge_2O_7$, and 0.03% In_2O_3. In order to see weak diffraction peaks, the y-scale is the square root of intensity. The dark blue points represent the measured diffracted intensity. The green line corresponds to the calculated intensities from Equation 2.3. The cyan line is the difference between the measured and fitted intensity, so a horizontal line would correspond to a perfect fit. The small vertical lines show the "d" positions of the diffraction peaks from each crystallographic phase in the sample.

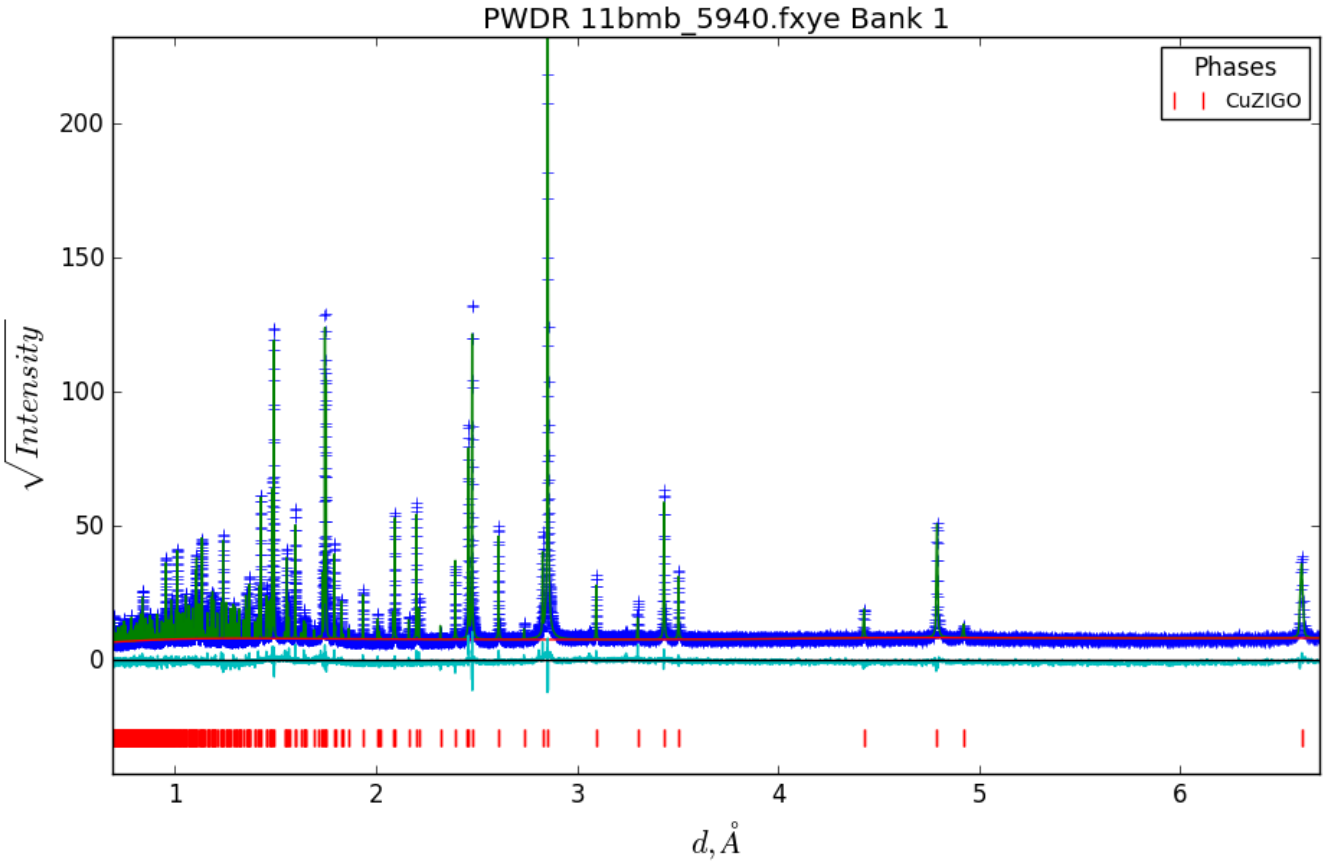

Figure 3.5: Rietveld refinement of XRD for $(Cu_xZn_{1-x})_{0.456}In_{1.084}Ge_{0.46}O_3$ sample x=0.75. Weak peaks have been found in the pattern, but have not been identified. In order to see weak diffraction peaks, the y-scale is the square root of intensity. The dark blue points represent the measured diffracted intensity. The green line corresponds to the calculated intensities from Equation 2.3. The cyan line is the difference between the measured and fitted intensity, so a horizontal line would correspond to a perfect fit. The small vertical lines show the "d" positions of the diffraction peaks from each crystallographic phase in the sample.

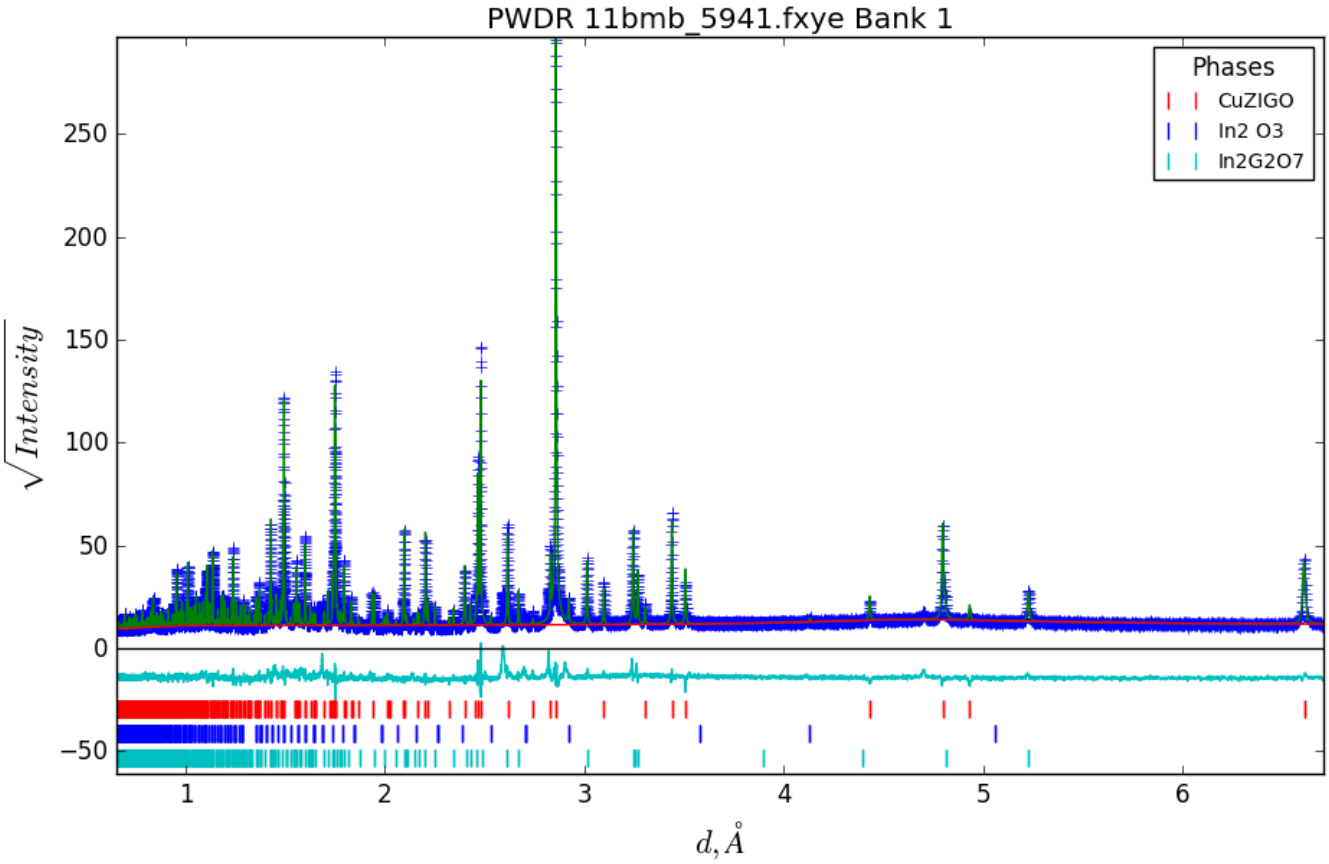

Figure 3.6: Rietveld refinement of XRD for $(Cu_xZn_{1-x})_{0.456}In_{1.084}Ge_{0.46}O_3$ sample x=1.00. The phase distribution is 93.3% CuZIGO, 6.4% $In_2Ge_2O_7$, and 0.3% In_2O_3. The same unidentified peaks found in the x=0.75 sample, were found in this pattern, but greater in strength. In order to see weak diffraction peaks, the y-scale is the square root of intensity. The dark blue points represent the measured diffracted intensity. The green line corresponds to the calculated intensities from Equation 2.3. The cyan line is the difference between the measured and fitted intensity, so a horizontal line would correspond to a perfect fit. The small vertical lines show the "d" positions of the diffraction peaks from each crystallographic phase in the sample.

Figures 3.3-3.6 give a visual representation of these refinements. The graphs display multiple blue plus markers which make up the graph of the measured intensities at each given d-spacing value. The green line is the calculated graph from the refined diffraction model. Ideally, the green line would match up exactly with the blue markers, if the analyzed diffraction data were perfect. However, there are some differences, and this can be seen in the cyan graph underneath. The graphs are plotted on a scale of the square root of intensity versus the d-spacing. The graphs have tick marks at the bottom to note the particular phase found at the given d-spacing values. For the x=0.25 sample, the peaks shown in Figure 3.3 represent the presence of three different phases at different d-spacing values. In Figures 3.5.3-7, however, there is evidence of unidentified peaks. These peaks are present where no phase is represented in the model. This shows that those samples have "unknown phases." These can be seen in Figure 3.7, most notably at the d-spacing values of $\sim$2.59, $\sim$2.82 and $\sim$2.90Å.

3.1.2 Refinements Exploring the Occupation of Cu at All Cation Sites

Additional refinements were run to determine if the 16f site is the most favorable site for copper to replace zinc. The first set of refinements for each sample involved keeping occupancies fixed at their ideal values, with copper only being substituted into the 16f site. The Uiso (isotropic atomic displacement parameter) values and atomic positions were also refined. The results of these refinements can be seen in Tables 3.1-3.4.

The next set of refinements involved fixing the Uiso values found in the first set of refinements. Copper was then included in the 4a, 4b and 8e sites in addition to the 16f site. A constraint was then placed for each sample limiting the total copper concentration. For the x=0.25 sample, the total copper was assumed to add up to 1.848. Presumably for x=0.50, total copper adds to 3.68, for x=0.75,

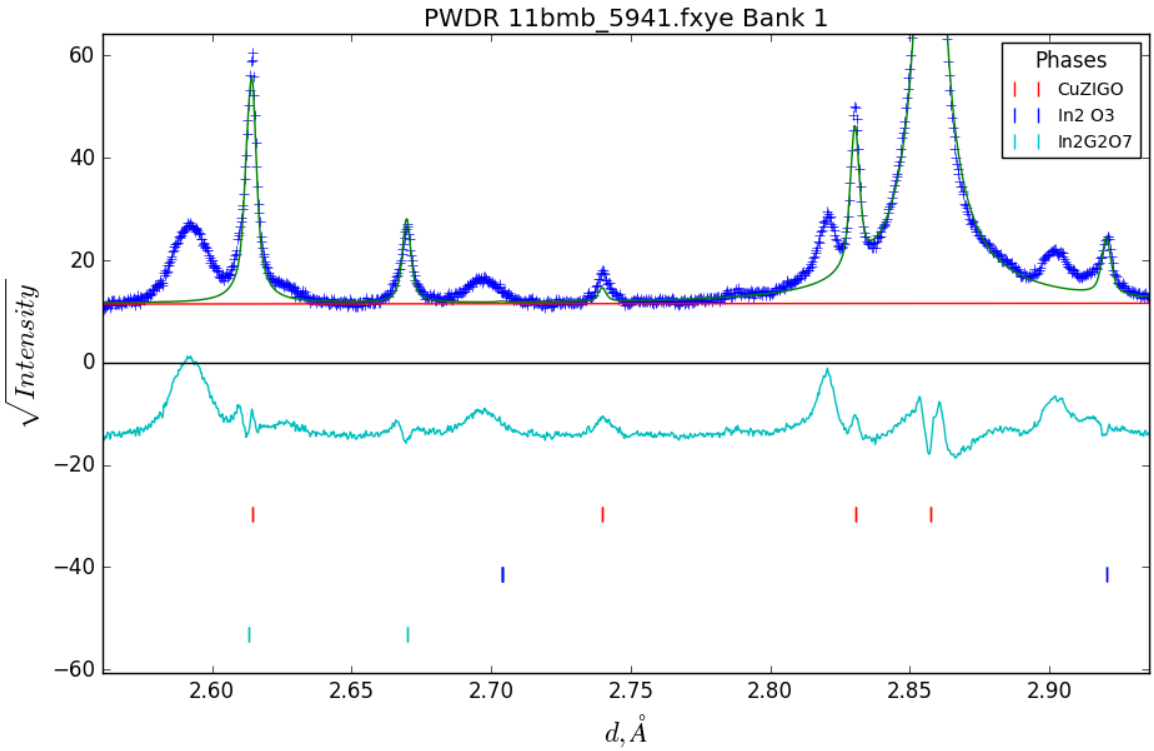

Figure 3.7: Zoomed in view of the unidentified peaks in the Rietveld refinement of XRD for $(Cu_xZn_{1-x})_{0.456}In_{1.084}Ge_{0.46}O_3$ sample x=1.00. These unidentified peaks cannot be indexed to CuZIGO, In_2O_3, or $In_2Ge_2O_7$ phases.

total copper adds to 5.512, and x=1.00 has a total copper amount equal to 7.36. These values were calculated using the copper concentrations of the powder mixtures and assuming there was no preferred volatilization. These concentrations were confirmed by an independent chemical analysis technique, ICP-OES (inductively coupled plasma-optical emission spectrometry).[12] The copper values in each site along with the indium found in the 4a and 8e sites and germanium found in the 4b site were all refined to identify if there was any possibility for copper to be substituted into these cation sites. This first trial for the x=0.25 sample, can be seen in Table S1. Noticeably, the copper occupancies in the 4a, 4b, and 8e sites all become negative during the refinement. This non-physical result suggests that

copper cannot be substituted into these sites. A similar result can be seen for the x=0.50, 0.75, and 1.00 samples in Tables S3, S6, and S9, respectively.

To further support the hypothesis, multiple refinements were run where this constraint refinement was combined with a refinement of the Uiso values and atomic positions. This was done to ensure that the negative occupancies are not just due to an inaccuracy in the placement of the atoms. This can be seen for each sample in Tables S2, S4, S7, and S10. For the x=0.25 sample in Table S2, similar to the result seen in Table S1, all occupancies continue to be negative. Table S10 displays the x=1.00 sample where copper in the 4a and 4b sites was found to be negative, and the occupancy in the 8e site was smaller than the uncertainty and thus assumed to be a negligible amount the site. Looking at the x=0.50 and 0.75 samples, only the 4b site was found to have negative occupancies for copper. In this case, a follow-up refinement was done to solidify the results. In the follow-up, the constraint was kept, but the copper that was originally in the 4b site was assumed to be zero. Then the constraint was updated so that the copper in the 4a, 8e, and 16f sites added up to 3.68 for the x=0.50 sample and 5.512 for the x=0.75 sample as seen in Tables S5 and S8. In both cases, the follow-up refinements led to negative occupancies in the 4a and 8e sites. These results support the hypothesis that the 16f site is the most favorable site.

Atom	Site	x	y	z	Occupancy	Uiso (Å)
In	4a	0	-0.25	0.125	1	0.0197(3)
In	8e	0.50	0.25	-0.10500(3)	1	0.0129(2)
Zn	16f	0.2272(1)	0	0	**0.344**	0.0218(2)
Cu					**0.116**	
In					**0.33**	
Ge					**0.21**	
Ge	4b	0.50	0.25	0.125	1	0.0148(4)
O1	16h	0	0.0287(8)	0.0723(2)	1	0.032(1)
O2	16h	0.50	0.0485(7)	0.0759(2)	1	0.033(2)
O3	16h	0.2547(7)	0.25	-0.0379(2)	1	0.044(2)

Table 3.1: Refinement results of the x=0.25 sample with Cu in only the 16f site with the atomic position and Uiso values were refined. Rw=10.605. Occupancies were fixed to values corresponding to the CuZIGO formula, $(Cu_xZn_{1-x})_{0.456}In_{1.084}Ge_{0.46}O_3$, where x=0.25,0.50, 0.75, and 1.00

Atom	Site	x	y	z	Occupancy	Uiso (Å)
In	4a	0	-0.25	0.125	1	0.0215(2)
In	8e	0.50	0.25	-0.10494(3)	1	0.0138(2)
Zn	16f	0.22726(8)	0	0	**0.23**	0.0220(2)
Cu					**0.23**	
In					**0.33**	
Ge					**0.21**	
Ge	4b	0.50	0.25	0.125	1	0.0144(3)
O1	16h	0	0.029(6)	0.07143(18)	1	0.026(1)
O2	16h	0.50	0.050(6)	0.0756(2)	1	0.037(1)
O3	16h	0.25351(62)	0.25	-0.0366(2)	1	0.046(1)

Table 3.2: Refinement results of the x=0.50 sample with Cu in only the 16f site with the atomic position and Uiso values were refined. Rw=10.091. Occupancies were fixed to values corresponding to the CuZIGO formula, $(Cu_xZn_{1-x})_{0.456}In_{1.084}Ge_{0.46}O_3$, where x=0.25,0.50, 0.75, and 1.00

Atom	**Site**	**x**	**y**	**z**	**Occupancy**	**Uiso (Å)**
In	4a	0	-0.25	0.125	1	0.0239(2)
In	8e	0.50	0.25	-0.10483(3)	1	0.0152(1)
Zn Cu In Ge	16f	0.22716(7)	0	0	**0.116** **0.344** **0.33** **0.21**	0.0232(1)
Ge	4b	0.50	0.25	0.125	1	0.0170(3)
O1	16h	0	0.02851(49)	0.07022(17)	1	0.0231(9)
O2	16h	0.50	0.0502(5)	0.0740(2)	1	0.041(1)
O3	16h	0.2543(6)	0.25	-0.0359(2)	1	0.047(1)

Table 3.3: Refinement results of the x=0.75 sample with Cu in only the 16f site with the atomic positions and Uiso values were refined. Rw=13.07. Occupancies were fixed to values corresponding to the CuZIGO formula, $(Cu_xZn_{1-x})_{0.456}In_{1.084}Ge_{0.46}O_3$, where x=0.25,0.50, 0.75, and 1.00

Atom	Site	x	y	z	Occupancy	Uiso (Å)
In	4a	0	-0.25	0.125	1	0.0226(3)
In	8e	0.50	0.25	-0.10523(4)	1	0.0162(2)
Zn	16f	0.22781(10)	0	0	**0**	0.0206(2)
Cu					**0.46**	
In					**0.33**	
Ge					**0.21**	
Ge	4b	0.50	0.25	0.125	1	0.0172(4)
O1	16h	0	0.0291(7)	0.07053(23)	1	0.026(1)
O2	16h	0.50	0.0487(7)	0.0734(2)	1	0.040(2)
O3	16h	0.2568(8)	0.25	-0.0358(3)	1	0.064(2)

Table 3.4: Refinement results of the x=1.00 sample with Cu in only the 16f site with the atomic positions and Uiso values were refined. Rw=13.965. Occupancies were fixed to values corresponding to the CuZIGO formula, $(Cu_xZn_{1-x})_{0.456}In_{1.084}Ge_{0.46}O_3$, where x=0.25,0.50, 0.75, and 1.00

3.1.3 Analysis of Neutron Data

As mentioned in Chapter 2, two x=0.25 and x=0.50 samples were synthesized to measure neutron diffraction data. Neutron data collected from the High Flux Isotope Reactor (HFIR) at Oak Ridge National Lab and from POWGEN, at the Spallation Neutron Source (SNS) were also refined. Rietveld refinements for neutron data were done using GSAS II. Similar to XRD data refinements, neutron data were originally refined using parameters similar to the x=0 sample to give a starting point for CuZIGO refinements. Similar to the XRD data, the best refinements involve copper being found only in the 16f site. This only gives further evidence that copper should only substitute into the 16f site. Figures 3.8 and 3.9 display the Rietveld refinements of the neutron data from HFIR. Similar to the XRD data displayed in Figures 3.3-3.6, these neutron refinements are graphed on the scale of square root of the intensity versus the d-spacing. They also have the teal graph displaying the difference between the expected and calculated graphs.

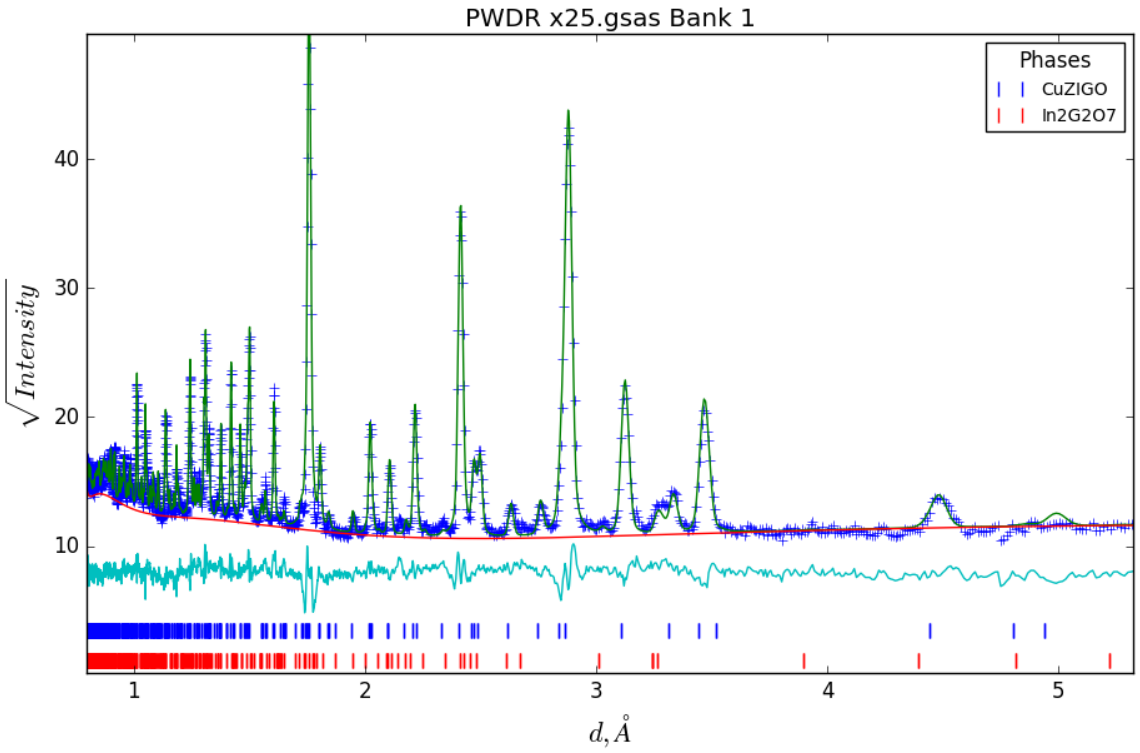

Figure 3.8: Rietveld refinement of ND for $(Cu_xZn_{1-x})_{0.456}In_{1.084}Ge_{0.46}O_3$ sample x=0.25. The phase distribution was found to be 98.9% CuZIGO, 1.1% $In_2Ge_2O_7$. In order to see weak diffraction peaks, the y-scale is the square root of intensity. The dark blue points represent the measured diffracted intensity. The green line corresponds to the calculated intensities from Equation 2.3. The cyan line is the difference between the measured and fitted intensity, so a horizontal line would correspond to a perfect fit. The small vertical lines show the "d" positions of the diffraction peaks from each crystallographic phase in the sample.

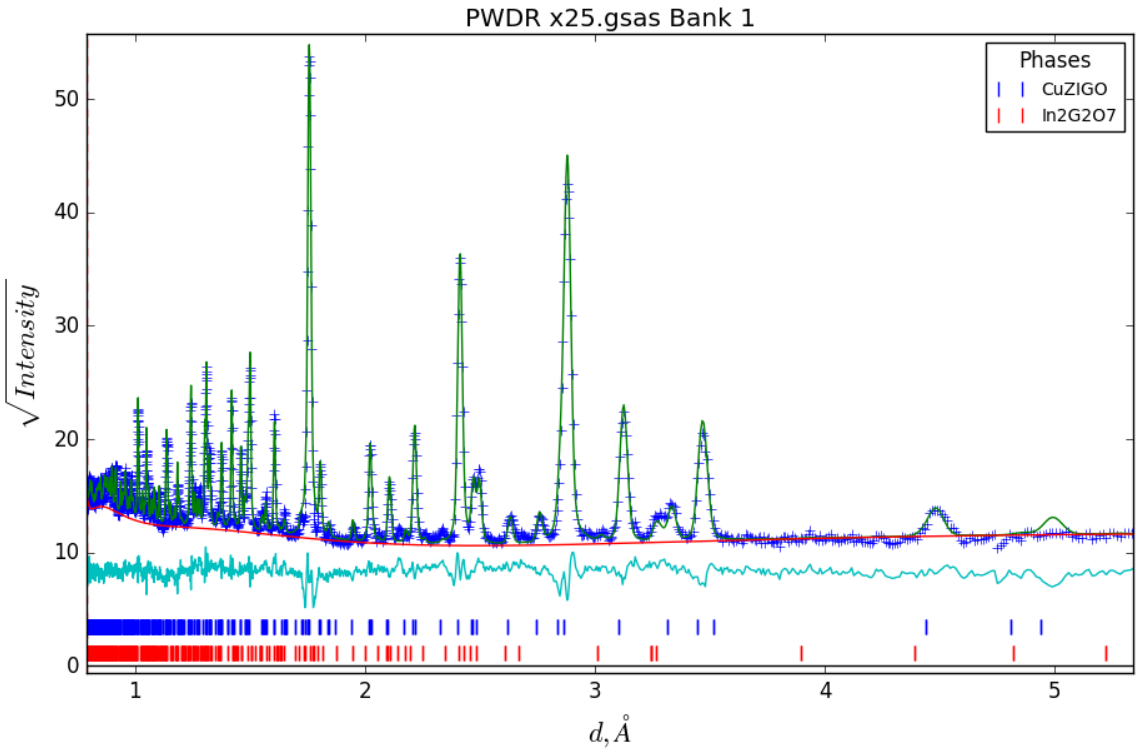

Figure 3.9: Rietveld refinement of ND for $(Cu_xZn_{1-x})_{0.456}In_{1.084}Ge_{0.46}O_3$ sample x=0.50. The phase distribution was found to be 98.8% CuZIGO, 1.2% $In_2Ge_2O_7$. In order to see weak diffraction peaks, the y-scale is the square root of intensity. The dark blue points represent the measured diffracted intensity. The green line corresponds to the calculated intensities from Equation 2.3. The cyan line is the difference between the measured and fitted intensity, so a horizontal line would correspond to a perfect fit. The small vertical lines show the "d" positions of the diffraction peaks from each crystallographic phase in the sample.

3.1.4 Challenges of Neutron Data Refinements

The neutron data produced some challenges when attempting the refinements of the occupations of all 4 cations at site 16f. This was not possible using only one data set. In order for the occupations of the 4 cations in the 16f site to all be fully refined, 3 independent diffraction patterns would be needed. Therefore, synchrotron data and another neutron diffraction pattern were collected at POWGEN on the same batch of samples. Once all 3 patterns were obtained, problems arose due to the presence of multiple CuZIGO phases. These phases affect the peak shape of the data leading to asymmetric peak shapes. Figures 3.10 and 3.11 show two zoomed in sections of the 3 diffraction patterns for the x=0.25 sample. These figures show the raw data for the intensities, without refinement, and displayed on the scale of Q-spacing. Q-spacing is related to d-spacing using the following equation:

$$Q = \frac{(2 * \pi)}{d} \tag{3.1}$$

The peaks are not matching due to sample displacement effects. If analyzed using the Rietveld refinement method, the displacement parameters would be refined, resulting in the same position for all 3 peaks.

In Figure 3.10, it is apparent that the resolution of the synchrotron data is much higher compared to that of HFIR and POWGEN. This is consistent with the instrumental resolution specifications given in Chapter 2. By looking at the ND data, one could conclude that there is just one diffraction peak from a single CuZIGO phase. However, the 11BM data from APS has a peak with a flat top, which is due to more than one CuZIGO phase. Expectedly, the peak would have just one maximum. Figure 3.11 shows a different section of the same diffraction patterns, with broad peaks corresponding to just one CuZIGO phase for the HFIR and POWGEN data. However, the 11-BM data shows splitting of peaks. This implies multiple phases of CuZIGO, which might be due to slightly different Cu amounts resulting in different lattice parameters.

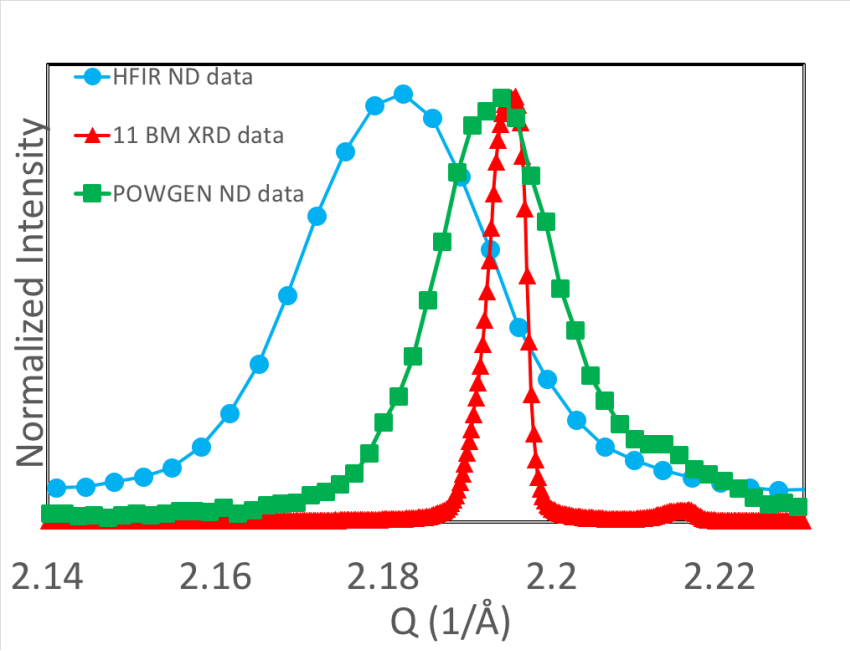

Figure 3.10: Resolution comparison of all 3 diffraction patterns from the XRD and neutron data for a large batch of the x=0.25 sample. The intensities were normalized for comparison purposes.

Multi-CuZIGO phases in the sample are attributed to the fact that several batches were prepared and combined to obtain more than 2 grams of sample for ND experiments. This problem was not encountered in the first series of samples that were only analyzed at 11-BM, since only a few micrograms are needed for those XRD experiments. Ideally if the sample was homogeneous and single-phase, a combined refinement of all 3 data sets (one XRD and two ND) would allow the occupational refinement of all 4 cations in site 16f. The presence of multiple CuZIGO phases in the samples prevented this combined refinement. Only the samples with single CuZIGO phases were then fully analyzed.

3.2 Bond Valence Analysis

The Cu occupation at only the 16f site in the CuZIGO structure can be backed up by knowledge gained from bond valence analysis (BVA). BVA shows that the 4b site is too small, and would cause significant over-bonding, even though it has the same tetrahedral structure as the 16f site.[12] The bond valence values listed in Table 3.5 are a measure of the strength of the bond between two given atoms. Using equation 3.2 for bond valence strengths, BVA can be used to determine the atom present in a particular site, such as the 4*b* site in Table 3.5.

$$S = \exp\left(R_0 - R\right)/B \tag{3.2}$$

In equation 3.2, S is the bond valence, R is the length of the bond between two atoms, R_0 is the parameter detailing the ideal bond length when the particular

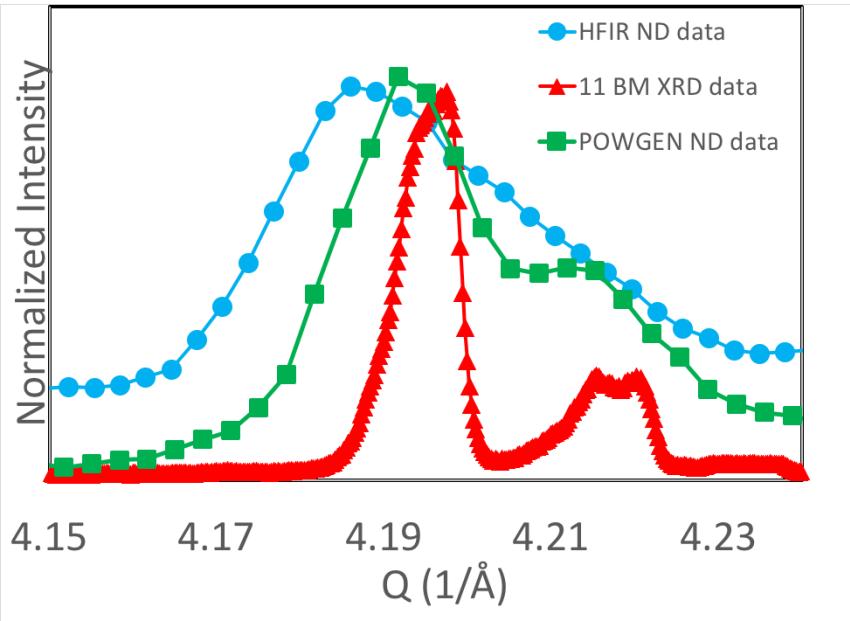

Figure 3.11: Resolution comparison of all 3 diffraction patterns form the XRD and neutron data for a large batch of the x=0.25 sample. The intensities were normalized for comparison purposes.

element has an exact valence of 1, and B is an empirical constant.[19] (These constants can be obtained from reference 17.) Given the distance between O^{2-} and the site, and using Equation 3.2, indium would require a charge >6, while copper and zinc would both be required to hold charges of >3, which is unrealistic for this particular system. However, when looking at germanium, the charge would need to be around 4, which is what is expected for this system. This gives evidence that the oxidation states for Cu found in the 16f site, are most closely matched to the expected value. Through refinement analysis and bond valence analysis, likelihood for the 4b and 8e sites has been diminished, and there is more support for the favoring of the 16f site.

Atom		**x=0.25**	**x=0.50**	**x=0.75**	**x=1.0**
4a‖	In	**2.55**	**2.52**	**2.48**	**2.40**
	Cu	1.39	1.38	1.35	1.31
	Zn	1.49	1.48	1.45	—
	Ge	1.68	1.66	1.63	1.58
16f‖	In	3.41	3.51	3.62	3.60
	Cu	1.86	1.92	**1.98**	**1.96**
	Zn	**1.99**	**2.05**	2.12	—
	Ge	2.24	2.31	2.38	2.36
8e‖	In	**3.06**	**2.95**	**2.89**	**2.94**
	Cu	1.67	1.61	1.58	1.60
	Zn	1.78	1.73	1.69	—
	Ge	2.01	1.94	1.90	1.93
4b‖	In	6.67	6.76	6.51	6.21
	Cu	3.64	3.69	3.55	3.39
	Zn	3.89	3.95	3.80	—
	Ge	**4.38**	**4.44**	**4.28**	**4.09**

Table 3.5: Bond Valence Analysis for X-ray Models. The bold values indicate the best match to the expected oxidation state.[12]

CHAPTER 4

Conclusion and Future Work

4.1 Conclusion

The present research studied the crystal structure of the solid solution $(Cu_xZn_{1-x})_{0.456}In_{1.084}Ge_{0.46}O_3$, which has promising optical and electrical properties. High-resolution synchrotron x-ray diffraction data on four powder samples with x=0.25, 0.50, 0.75, and 1.00 compositions were collected and analyzed. Rietveld refinement results determined that all samples crystallize in the tetragonal $I4_1/amd$ structure, similarly to the x=0, ZIGO phase. This structure has 4 cation sites (4a, 4b, 8e, and 16f) and 3 anion sites (16h) where oxygen is found. Indium fully occupies the 4a and 8e sites. Only germanium is present at the 4b site. Zinc, indium, germanium, and copper occupy the 16f site.

The diffraction results show that copper only substitutes for zinc in the 16f site. As evidenced in Tables 3.1-3.4 and Tables S1-S10, analyses with copper being substituted into the other sites all resulted in non-physical refinements. In the end, a complete solid solution between copper and zinc was found in the tetragonal ZIGO structure. As copper was incorporated into the ZIGO structure, both lattice parameters decreased, except for the x= 1.00 endpoint composition. The changes in lattice parameter show that a full solid solution was obtained.

As the search for new materials and properties continues, quaternary phases are becoming increasingly relevant due to the already thorough exploration of binary and ternary compounds. This project looked at a transparent conducting oxide that could start an exploration of a new branch of complex structures. Looking

at CuZIGO opens the door for new p-type semiconductors, which expands and complements the applications of the n-type TCOs that are better known currently.

Looking to the future, one plan is to study other quaternary phase compounds. The possibilities of CuZIGO may prompt further study of other complex structures, such as mixed anion materials including oxyfluorides, which could have different properties and applications. The complexity of characterizing quaternary compounds is challenging, as evidenced by this study. Ideally, refinements with XRD and two ND data sets would be measured and analyzed on single-phase samples to get more accurate results on these types of materials. This information gives a better understanding of current compounds and aids in the design of new materials.

APPENDIX

Atom	Site	x	y	z	Occupancy	Uiso (Å)
In Cu	4a	0	-0.25	0.125	**1.045(8)** **-0.045(3)**	0.01972
In Cu	8e	0.50	0.25	-0.10491(3)	**1.026(7)** **-0.026(7)**	0.01285
Zn Cu In Ge	16f	0.2271(1)	0	0	**0.344** **0.159(4)** **0.33** **0.21**	0.02176
Ge Cu	4b	0.50	0.25	0.125	**1.080(3)** **-0.080(3)**	0.01480
O1	16h	0	0.0290(7)	0.0725(2)	1	0.03155
O2	16h	0.50	0.0489(7)	0.0762(2)	1	0.03334
O3	16h	0.2551(8)	0.25	-0.0381(2)	1	0.04355

Table S1: Refinement results of the x=0.25 sample with Cu in the 4a, 8e, 4b and 16f sites with copper occupancies refined, but with total fractional value between all sites with copper constrained to equal 1.848. Atomic positions are also refined. Rw=10.57. Negative occupancies and occupancies greater than one indicate that the model is non physical.

Atom	Site	x	y	z	Occupancy	Uiso (Å)
In Cu	4a	0	-0.25	0.125	**1.03(2)** **-0.03(2)**	0.0196(4)
In Cu	8e	0.50	0.25	-0.10500(3)	**1.05(1)** **-0.05(1)**	0.01360(3)
Zn Cu In Ge	16f	0.2273(1)	0	0	**0.344** **0.173** **0.33** **0.21**	0.0243(3)
Ge Cu	4b	0.50	0.25	0.125	**1.14(5)** **-0.14(5)**	0.0148(7)
O1	16h	0	0.081(8)	0.0733(3)	1	0.027(1)
O2	16h	0.50	0.0489(7)	0.0763(2)	1	0.029(2)
O3	16h	0.2546(8)	0.25	-0.0384(2)	1	0.036(2)

Table S2: Refinement results of x=0.25 with Cu in the 4a, 8e, 4b, and 16f sites with total fractional value between all sites with copper constrained to equal 1.848. Uiso values and atomic positions are also refined. Rw=10.79. Negative occupancies and occupancies greater than one indicate that the model is non physical.

Atom	Site	x	y	z	Occupancy	Uiso (Å)
In Cu	4a	0	-0.25	0.125	**0.978(6)** **0.022(6)**	0.02149
In Cu	8e	0.50	0.25	-0.10486(3)	**0.991(6)** **0.009(6)**	0.01382
Zn Cu In Ge	16f	0.22721(8)	0	0	**0.23** **0.249(3)** **0.33** **0.21**	0.02201
Ge Cu	4b	0.50	0.25	0.125	**1.12(2)** **-0.12(2)**	0.01444
O1	16h	0	0.0285(6)	0.0719(2)	1	0.02582
O2	16h	0.50	0.0501(6)	0.0756(2)	1	0.03730
O3	16h	0.2536(6)	0.25	-0.0369(2)	1	0.04598

Table S3: Refinement results of the x=0.50 sample with Cu in the 4a, 8e, 4b and 16f sites with copper occupancies refined, but with total fractional value between all sites with copper constrained to equal 3.68. Atomic positions are also refined. Rw=10.071. Negative occupancies and occupancies greater than one indicate that the model is non physical.

Atom	Site	x	y	z	Occupancy	Uiso (Å)
In Cu	4a	0	-0.25	0.125	**0.93(1)** **0.07(1)**	0.0188(3)
In Cu	8e	0.50	0.25	-0.10493(3)	**0.98(1)** **0.02(1)**	0.0128(2)
Zn Cu In Ge	16f	0.22732(8)	0	0	**0.23** **0.273(5)** **0.33** **0.21**	0.0239(2)
Ge Cu	4b	0.50	0.25	0.125	**1.29(4)** **-0.29(4)**	0.0171(5)
O1	16h	0	0.0279(6)	0.0724(2)	1	0.024(1)
O2	16h	0.50	0.0499(6)	0.0756(2)	1	0.036(1)
O3	16h	0.2533(6)	0.25	-0.0372(2)	1	0.043(2)

Table S4: Refinement results of the x=0.50 sample with Cu in the 4a, 8e, 4b and 16f sites with copper occupancies refined, but with total fractional value between all sites with copper constrained to equal 3.68. Uiso values and atomic positions are also refined. Rw=10.061. Negative occupancies and occupancies greater than one indicate that the model is non physical.

Atom	Site	x	y	z	Occupancy	Uiso (Å)
In Cu	4a	0	-0.25	0.125	**1.154(3)** **-0.154(3)**	0.0226(3)
In Cu	8e	0.50	0.25	-0.10494(3)	**1.08(7)** **-0.08(1)**	0.0123(2)
Zn Cu In Ge	16f	0.22744(8)	0	0	**0.23** **0.306(3)** **0.33** **0.21**	0.0240(2)
Ge Cu	4b	0.50	0.25	0.125	1 0	0.0116(3)
O1	16h	0	0.0302(6)	0.0719(2)	1	0.022(1)
O2	16h	0.50	0.0518(6)	0.0764(2)	1	0.031(1)
O3	16h	0.2553(6)	0.25	-0.0370(2)	1	0.035(1)

Table S5: Refinement results of the x=0.50 sample with Cu in the 4a, 8e, and 16f sites with copper occupancies refined, but with total fractional value between all sites with copper constrained to equal 3.68. Uiso values and atomic positions are also refined. Rw=10.156. Negative occupancies and occupancies greater than one indicate that the model is non physical.

Atom	Site	x	y	z	Occupancy	Uiso (Å)
In Cu	4a	0	-0.25	0.125	**0.985(6)** **0.015(6)**	0.02391
In Cu	8e	0.50	0.25	-0.10479(2)	**0.992(5)** **0.008(5)**	0.01521
Zn Cu In Ge	16f	0.22714(7)	0	0	**0.116** **0.357(3)** **0.33** **0.21**	0.02320
Ge Cu	4b	0.50	0.25	0.125	**1.08(2)** **-0.08(2)**	0.01695
O1	16h	0	0.0286(5)	0.0706(2)	1	0.02310
O2	16h	0.50	0.0503(5)	0.0742(2)	1	0.04110
O3	16h	0.2545(6)	0.25	-0.0361(2)	1	0.04669

Table S6: Refinement results of the x=0.75 sample with Cu in the 4a, 8e, 4b and 16f sites with copper occupancies refined, but with total fractional value between all sites with copper constrained to equal 5.512. Atomic positions are also refined. Rw=13.051. Negative occupancies and occupancies greater than one indicate that the model is non physical.

Atom	Site	x	y	z	Occupancy	Uiso (Å)
In Cu	4a	0	-0.25	0.125	**0.98(1)** **0.02(1)**	0.0231(3)
In Cu	8e	0.50	0.25	-0.10482(3)	**0.981(8)** **0.019(8)**	0.0144(2)
Zn Cu In Ge	16f	0.22719(8)	0	0	**0.116** **0.375(4)** **0.33** **0.21**	0.0243(2)
Ge Cu	4b	0.50	0.25	0.125	**1.18(4)** **-0.18(4)**	0.018(5)
O1	16h	0	0.0287(5)	0.0706(2)	1	0.0218(9)
O2	16h	0.50	0.0500(6)	0.0742(2)	1	0.039(1)
O3	16h	0.2548(6)	0.25	-0.0362(2)	1	0.044(1)

Table S7: Refinement results of the x=0.75 sample with Cu in the 4a, 8e, 4b and 16f sites with copper occupancies refined, but with total fractional value between all sites with copper constrained to equal 5.512. Uiso values and atomic positions are also refined. Rw=13.068. Negative occupancies and occupancies greater than one indicate that the model is non physical.

Atom	Site	x	y	z	Occupancy	Uiso (Å)
In Cu	4a	0	-0.25	0.125	**1.097(3)** **-0.097(3)**	0.0246(2)
In Cu	8e	0.50	0.25	-0.10483(2)	**1.046(5)** **-0.046(5)**	0.0143(2)
Zn Cu In Ge	16f	0.22722(7)	0	0	**0.116** **0.392(3)** **0.33** **0.21**	0.0244(2)
Ge Cu	4b	0.50	0.25	0.125	1 0	0.0153(3)
O1	16h	0	0.0296(5)	0.0706(2)	1	0.0210(9)
O2	16h	0.50	0.0512(5)	0.0747(2)	1	0.037(1)
O3	16h	0.2554(6)	0.25	-0.0363(2)	1	0.040(1)

Table S8: Refinement results of the x=0.75 sample with Cu in the 4a, 8e, and 16f sites with copper occupancies refined, but with total fractional value between all sites with copper constrained to equal 5.512. Uiso values and atomic positions are also refined. Rw=13.087. Negative occupancies and occupancies greater than one indicate that the model is non physical.

Atom	Site	x	y	z	Occupancy	Uiso (Å)
In Cu	4a	0	-0.25	0.125	**1.021(8)** **-0.02(6)**	0.02254
In Cu	8e	0.50	0.25	-0.10514(3)	**0.995(7)** **0.005(7)**	0.01618
Zn Cu In Ge	16f	0.2278(1)	0	0	**0** **0.49(4)** **0.33** **0.21**	0.02067
Ge Cu	4b	0.50	0.25	0.125	**1.11(3)** **-0.11(3)**	0.01714
O1	16h	0	0.0301(7)	0.0710(3)	1	0.02642
O2	16h	0.50	0.0489(7)	0.0737(3)	1	0.03986
O3	16h	0.2580(8)	0.25	-0.0364(3)	1	0.06388

Table S9: Refinement results of the x=1.00 sample with Cu in the 4a, 8e, 4b and 16f sites with copper occupancies refined, but with total fractional value between all sites with copper constrained to equal 7.36. Atomic positions are also refined. Rw=13.914. Negative occupancies and occupancies greater than one indicate that the model is non physical.

Atom	Site	x	y	z	Occupancy	Uiso (Å)
In Cu	4a	0	-0.25	0.125	**1.02(1)** **-0.02(1)**	0.0212(4)
In Cu	8e	0.50	0.25	-0.10526(4)	**0.998(3)** **0.002(3)**	0.0141(2)
Zn Cu In Ge	16f	0.2278(1)	0	0	**0** **0.515(6)** **0.33** **0.21**	0.0233(2)
Ge Cu	4b	0.50	0.25	0.125	**1.20(3)** **-0.20(3)**	0.0176(5)
O1	16h	0	0.0304(7)	0.0714(3)	1	0.024(1)
O2	16h	0.50	0.0491(8)	0.0739(3)	1	0.037(2)
O3	16h	0.2586(8)	0.25	-0.0367(3)	1	0.054(2)

Table S10: Refinement results of the x=1.00 sample with Cu in the 4a, 8e, 4b and 16f sites with copper occupancies refined, but with total fractional value between all sites with copper constrained to equal 7.36. Uiso values and atomic positions are also refined. Rw=13.876. Negative occupancies and occupancies greater than one indicate that the model is non physical.

REFERENCES

[1] Stadler, Andreas., Transparent Conducting Oxides—An Up-To-Date Overview. *Materials (Basel)*, **2012**, *5*(12), 661–683.

[2] Edwards, P. P., *et al.*, Basic Materials Physics of Transparent Conducting Oxides. *Dalton Transactions*,**2004**, *19*, 2995-3002.

[3] Coutts, T J, *et al.*, Transparent Conducting Oxides: Status and Opportunities in Basic Research. *U.S. Department of Energy*, **1999**.

[4] Chen, Z., Li, W., Li, R., Zhang, Y., Xu, G., Cheng, H. Fabrication of Highly Transparent and Conductive Indium–Tin Oxide Thin Films with a High Figure of Merit via Solution Processing. *Langmuir.* **2013**, *29(45)*; 13836-13842

[5] Rickert, K.; Sedefoglu, N.; Malo, S.; Caignaert, V.; Kavak, H.; Poeppelmeier, K. R.; Structural, Electrical, and Optical Properties of the Tetragonal, Fluorite-Related $Zn_{0.456}In_{1.084}Ge_{0.46}O_3$. *Chem Mater.* **2015**, *27*(14), 5072-5079.

[6] González, G.B.; Studies on the Defect Structure of Indium-Tin Oxide Using X-ray and Neutron Diffraction. *Ph.D. Dissertation, Northwestern University, Evanston, IL, USA*, **2003**.

[7] Wyckoff Position. Wyckoff Position-Online Dictionary of Crystallography, *International Union of Crystallography.*

[8] González, G. B.; Investigating the Defect Structures in Transparent Conducting

Oxides Using X-ray and Neutron Scattering Techniques. *Materials.* **2012**, *5*; 818-850.

[9] Sheng, S *et al.* P-Type Transparent Conducting Oxides, *Phys. Status Solidi* **2006**, *203*(8), 1891–1900.

[10] Sohn, Sunyoung, Soo Han, Yoon; Transparent Conductive Oxide (TCO) Films for Organic Light Emissive Devices (OLEDs). *Organic Light Emitting Diode – Material, Process and Devices* **2011**, 233-274.

[11] Sugiura, Toshifumi. Barrier Potential across Semiconductor P-N Junction and Resting Membrane Potential. *Journal of Arrhythmia.* **2011**, *27.* 353–355.

[12] Flynn, S., Adekoya, A., Saeed, S., Zhang, C., Dravid V. P., González, G. B., and Poeppelmeier, K.R.; $(Cu_xZn_{1-x})_{0.456}In_{1.084}Ge_{0.46}O_3$: $(0 \leq x \leq 1)$: A Complex, Ordered, Anion-Deficient Fluorite with Unusual Site-Specific Cation Mixing. *Inorganic Chemistry.* **2019**.

[13] Rodriguez-Carvajal, J. FULLPROF: a program for Rietveld refinement and pattern matching analysis. *Physica B.*, **1993**, *192*, 55.

[14] Toby, B. H., Von Dreele, R. B., GSAS-II: the genesis of a modern open-source all purpose crystallography software package. *Journal of Applied Crystallography*, **2013**, *46(2)*, 544-549.

[15] Rietveld, H.M.; A profile refinement method for nuclear and magnetic structure, *J. Appl. Crystallogr.* **1969**, *2*, 65–71.

[16] Nix, R. Miller Indices (hkl); *Chemistry Libre Texts.* **2019**.

[17] The Editors of Encyclopaedia Britannica. Miller indices; *Encyclopædia Britannica*, **2018**.

[18] Denton, A. R.; N. W. Ashcroft. Vegard's Law. *Phys. Rev. A: At Mol., Opt. Phys.* **1991**, *43*; 3161–3164.

[19] Brown, I.D. The Chemical Bond In Inorganic Chemistry: The Bond Valence Model; *Oxford University Press.* **2016**, *27*.

Acknowledgements

I would like to thank Dr. Gabriela González Avilés for her help and support throughout the research and writing process of this thesis. I would also like to thank the faculty and staff of the DePaul University Physics Department for their support throughout this process, especially those involved in my thesis committee, Dr. Anuj Sarma and Dr. Bernhard Beck-Winchatz.

I would like to thank our collaborators in the Northwestern University Materials Research Science and Engineering Center, in particular, those involved in the IRG-2 and my direct work with Steven Flynn and Dr. Ken Poeppelmeier, who prepared the samples. NSF-MRSEC grant number DMR-1720139 funded this research.

This x-ray diffraction data were collected at 11BM of the Advanced Photon Source, a U.S. Department of Energy (DOE) Office of Science User Facility operated for the DOE Office of Science by Argonne National Laboratory under contract No. DE-AC02-06CH11357. This research also used resources at the High Flux Isotope Reactor and the Spallation Neutron Source, a DOE Office of Science User Facilities operated by Oak Ridge National Laboratory. Stuart A. Calder collected the neutron diffraction data at the HB-2A diffractometer of HFIR. The SNS data were collected via the mail-in program at the POWGEN beamline. Brian Toby and Robert Von Dreele provided valuable guidance in the Rietveld refinements.